Supporting Information for

Lanthanide complex-based dual-modal probes for background-free time-gated luminescence and ^{19}F magnetic resonance detection of hypochlorous acid in acute kidney injury

Shuqi Duan,[a] Qi Liu,[a] Xinyue Zhang,[a] Wenzhu Zhang,[a] Jingli Yuan [b] and Bo Song,*[a]

[a] School of Chemistry, Dalian University of Technology, Dalian 116024, China.

[b] College of Life Science, Dalian Minzu University, Dalian 116600, China.

*Corresponding authors

E-mail: bo.song@dlut.edu.cn

Table of Contents

1. Experiment Section

1.1 Materials

Sodium hypochlorite (NaClO), Europium(III) chloride hexahydrate ($EuCl_3 \cdot 6H_2O$), gadolinium(III) chloride hexahydrate ($GdCl_3 \cdot 6H_2O$), cisplatin, L-carnitine (LC), sodium trifluoromethanesulfonate, heptafluorobutyric acid, and 3-(4,5-dimethylthiazol-2-yl)-2,5-diphenyltetrazolium bromide (MTT) were purchased from Aladdin Reagent Co., Ltd. (Shanghai, China). Urea nitrogen and creatinine assay kits were purchased from Nanjing Jiancheng Bioengineering Institute (China). An isotonic saline solution (ISS) consisting of 140 mM NaCl, 10 mM glucose, and 3.5 mM KCl was prepared in our laboratory. HeLa cells and HK-2 cells were obtained from Dalian Medical University. All chemicals and reagents were obtained from commercial suppliers and used as received without further purification. Deionized water was used throughout the entire process. All experiments were performed in accordance with relevant laws and institutional guidelines. All animal experiments were conducted in compliance with procedures approved by the Animal Care and Use Committee of Dalian Medical University.

1.2 Physical measurements

^{1}H NMR, ^{13}C NMR, and ^{19}F NMR spectra were measured on a Bruker Avance 400 spectrometer. UV-vis absorption spectra were measured on a Shimadzu UV-1800 UV spectrophotometer with a 1.0 cm quartz cell. Mass spectra were measured on an HP1100 LC/MSD instrument. Dynamic light scattering (DLS) data were acquired on a Litesizer™ 500 500 instrument (Anton Paar). Time-gated luminescence (TGL) spectra were recorded on a Perkin Elmer LS 50B luminescence spectrometer. Luminescence lifetimes were measured on an Edinburgh FS5 spectrofluorometer. TGL imaging experiments were performed on a true-color TGL microscope developed in our laboratory.[1] The *ex vivo* imaging of mouse organs was performed on a MIIS XFP-BIX multifunctional *in vivo* imager (Molecular Devices, San Jose, USA).

1.3 Preparation of different analytes

Stock solutions (10.0 mM) of anions (NO_2^- and NO_3^-) and biological small molecules (Vitamin C, Hcy, GSH, and Cys) were prepared by dissolving sodium nitrite ($NaNO_2$), sodium nitrate ($NaNO_3$), Vitamin C, homocysteine (Hcy), glutathione (GSH), and cysteine (Cys) in deionized water, respectively.

For reactive oxygen species (ROS) and reactive nitrogen species (RNS): H_2O_2 and TBHP were prepared by diluting commercial 30% H_2O_2 and 70% *tert*-butyl hydroperoxide (TBHP) solutions with deionized water, respectively. Superoxide anion ($O_2^{\bullet-}$) was generated by dissolving potassium superoxide (KO_2) in anhydrous DMSO. Hydroxyl radical (•OH) was generated by the Fenton reaction between Fe^{2+} (1.0 mM) and H_2O_2 (100 μM). Singlet oxygen ($^1O_2$) was generated by the reaction of Na_2MoO_4 with H_2O_2. Nitric oxide (NO) was generated by dissolving sodium nitroprusside (SNP) in deionized water. For the specificity assays, the final concentration of all interfering species in the testing system was maintained at 100 μM.

1.4 Spectroscopic Response of Eu(SDHH)$_3$(DPBT) to HClO

The HClO solution was prepared by diluting a commercial sodium hypochlorite (NaClO) solution with deionized water, and its concentration was determined by measuring the absorbance at 292 nm ($\varepsilon_{292\ nm}$ = 350 M^{-1} cm^{-1}). For spectroscopic studies, the probe Eu(SDHH)$_3$(DPBT) (5 μM) was incubated with different concentrations of HClO in borate buffer (50 mM, pH 7.4) at 37 °C for 5 min. Subsequently, the time-gated luminescence (TGL) emission spectra were recorded on a Perkin Elmer LS 50B spectrometer with an excitation wavelength of 405 nm. The instrument settings were as follows: delay time, 0.2 ms; gate time, 0.4 ms; cycle time, 20 ms; excitation slit, 7 nm; and emission slit, 7 nm. For selectivity and competition assays, the probe was treated with HClO (50 μM) or other analytes (100 μM) under the same conditions.

1.5 Detection limit:

The detection limit (LOD = $3\sigma/k$) was calculated based on the linear relationship between the TGL intensity at 607 nm and the concentration of HClO. σ is the standard deviation of the blank measurement (n = 10) and k is the slope of the TGL intensity versus HClO concentration.

1.6 Statistical Analysis

All quantitative data are expressed as the mean ± standard deviation (SD). The assumption of homoscedasticity was assessed using the Brown-Forsythe test. Due to unequal variances across groups, statistical significance for multiple comparisons was determined using Welch's ANOVA followed by Dunnett's T3 post-hoc test. Comparisons between two independent groups were performed using an unpaired, two-tailed Welch's t-test. A P value < 0.05 was considered statistically significant (* $P < 0.05$, ** $P < 0.01$, *** $P < 0.001$, **** $P < 0.0001$).

1.7 Water solubility investigation

Saturated aqueous solutions of **$Eu(SDHH)_3(DPBT)$** and **$Eu(DHH)_3(DPBT)$** were prepared in deionized water. Briefly, excess solids were added to deionized water and stirred at 25 °C for 24 h to ensure saturation. The suspensions were filtered through a 0.45 μm syringe filter to remove undissolved particles. The clear filtrates were then analyzed by UV-vis absorption spectroscopy. Additionally, the luminescence brightness of the solutions was visually compared under a 365 nm UV lamp. Higher absorbance and luminescence intensity in the saturated solution directly correlates to higher water solubility based on the Beer-Lambert law.

1.8 Cell culture and cytotoxicity assay

HeLa cells were cultured in Dulbecco's Modified Eagle Medium (DMEM), while HK-2 cells were maintained in DMEM/F-12 medium. Both media were supplemented with 10% fetal bovine serum (FBS), 1% penicillin, and 1% streptomycin. The cells were incubated in a humidified atmosphere containing 5% CO_2 at 37 °C. The cytotoxicity of **$Eu(SDHH)_3(DPBT)$** was detected by the MTT colorimetric assay: cells were seeded in 96-well plates at a density of 5×10^3 cells per well and cultured for 24 h, followed by incubation with the probe at various concentrations (0, 10, 20, 40, 60, 80 μM) for another 24 h; 100 μL of MTT solution (0.5 mg/mL) was added to each well, and after further incubation for 4 h, the supernatant was discarded; 100 μL of dimethyl sulfoxide (DMSO) was added to each well to dissolve the formazan crystals; the absorbance of the solution at 490 nm was measured using an Infinite M200 Pro Microplate Reader. The results of five independent experiments were averaged, and the cell viability was calculated using the following formula:

Viability (%) = (mean of absorbance value of treatment group-blank) / (mean absorbance value of control-blank) × 100.

1.9 Determination of Luminescence Quantum Yield

For determining the luminescence quantum yields of $Eu(SDHH)_3(DPBT)$, the reported Eu^{3+} complex, 4'-phenyl-2,2':6',2"-terpyridine-6,6"-bis(methylenenitrilo) tetrakis(acetic acid)-Eu^{3+} (PTTA-Eu^{3+}) was employed as a reference standard ($\phi_2 = 0.160$). The luminescence quantum yield of the lanthanide complex probe (ϕ_1) was calculated by using the equation:

$$\phi_1 = I_1\varepsilon_2\phi_2C_2/I_2\varepsilon_1C_1$$

In this equation: I_1 and I_2, ε_1 and ε_2, C_1 and C_2 are the luminescence intensities, molar extinction coefficients, and concentrations for the measured complex and the standard complex, respectively.

2. Synthesis and Characterization of Intermediate Compounds and Ligands SDHH and DPBT

2.1 Synthesis of SDHH and DPBT

The reaction pathway for the synthesis of SDHH is illustrated in Scheme S1. The precursor CDHH of SDHH was synthesized according to a previously reported method.[2]

Synthesis of 4'-(4,4,5,5,6,6,6-heptafluoro-3-oxohexanoyl)-[1,1'-biphenyl]-4-sulfonic acid (SDHH). CDHH (500 mg, 1.02 mmol) was dissolved in DMSO (1 mL) under ultrasonication. Subsequently, deionized water (10 mL) was added, and the mixture was stirred for 12 h. The product was collected by centrifugation, washed with a small amount of water, and freeze-dried overnight to affording SDHH as a milky white solid (272 mg, yield: 54.4%). ^{1}H NMR (400 MHz, DMSO-*d6*) δ (ppm)= 8.24 (d, *J* = 8.0 Hz, 2H), 7.91 (d, *J* = 8.0 Hz, 2H), 7.75 (q, *J* = 8.0 Hz, 4H), 7.10 (s, 1H). ^{13}C NMR (101 MHz, DMSO-d_6) δ(ppm) = 184.61, 176.29, 176.04, 175.78, 148.52, 145.42, 138.37, 131.20, 128.90, 127.30, 126.52, 126.33, 94.39. ESI-MS (m/z): 470.86 $[M-H]^-$.

Synthesis of 4-(4,6-bis(3,5-dimethyl-1H-pyrazol-1-yl)-1,3,5-triazin-2-yl)-N,N-diethylaniline (DPBT). The synthesis of DPBT was carried out using a known method.[3] ^{1}H NMR (400 MHz, Chloroform-*d*) δ(ppm) = 8.50 (s, 2H), 7.22 – 6.67 (m, 2H), 6.11 (s, 2H), 3.50 (d, *J* = 8.0 Hz, 4H), 2.86 (s, 6H), 2.36 (s, 6H), 1.26 (t, *J* = 7.2 Hz, 6H). ESI-MS (m/z): 439.10 $[M+Na]^+$.

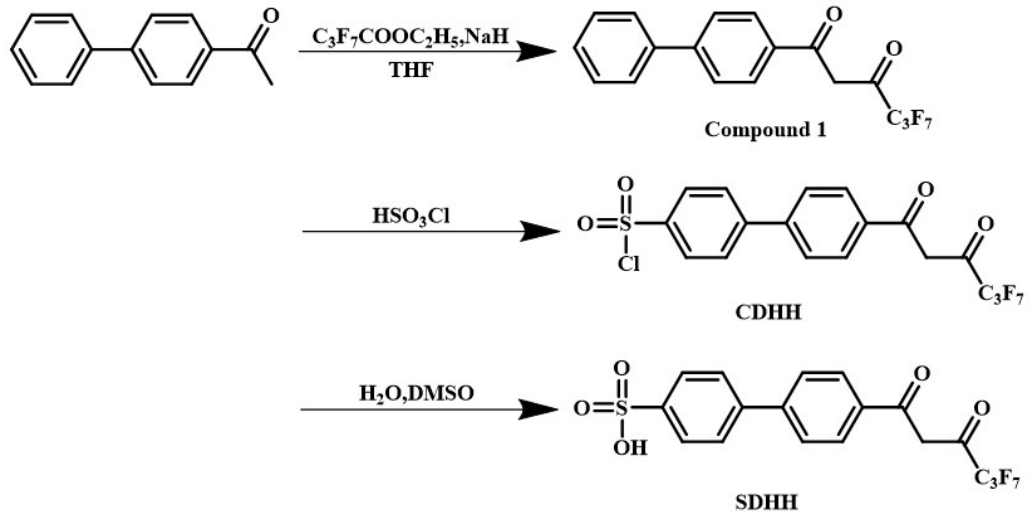

Scheme S1. Reaction pathway for the synthesis of SDHH.

2.2 Characterization of the intermediate compounds and the ligands

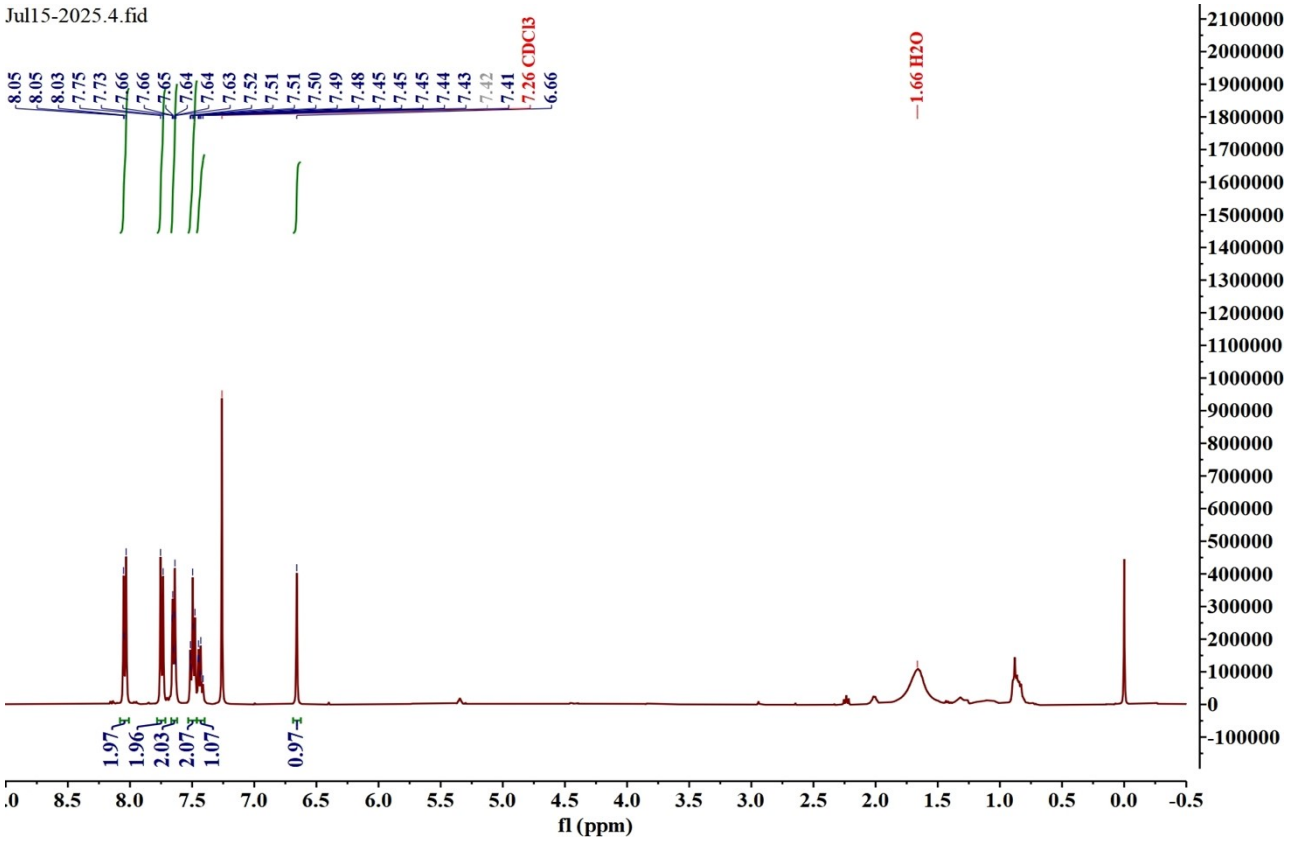

Figure S1. ^{1}H NMR spectrum of compound 1 in $CDCl_3$.

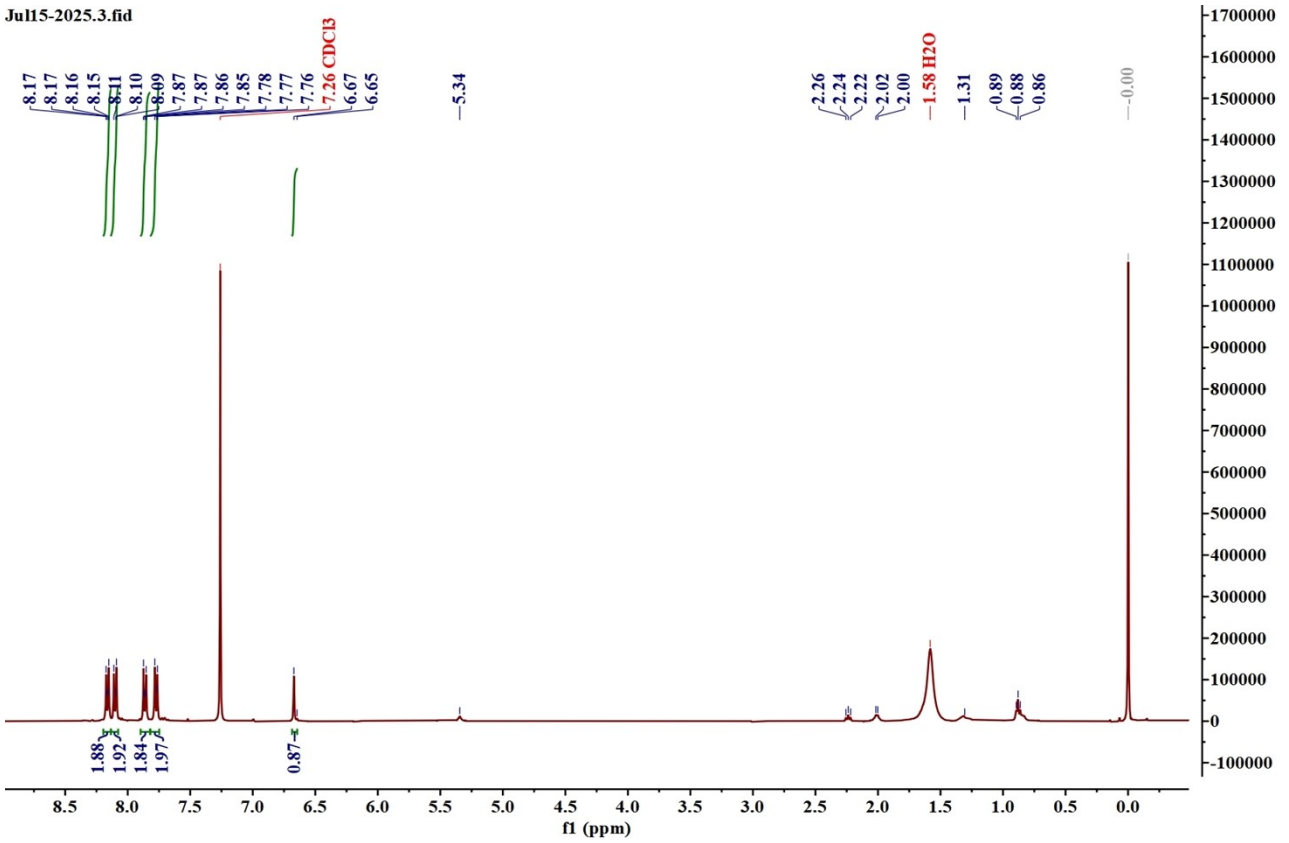

Figure S2. ^{1}H NMR spectrum of CDHH in $CDCl_3$.

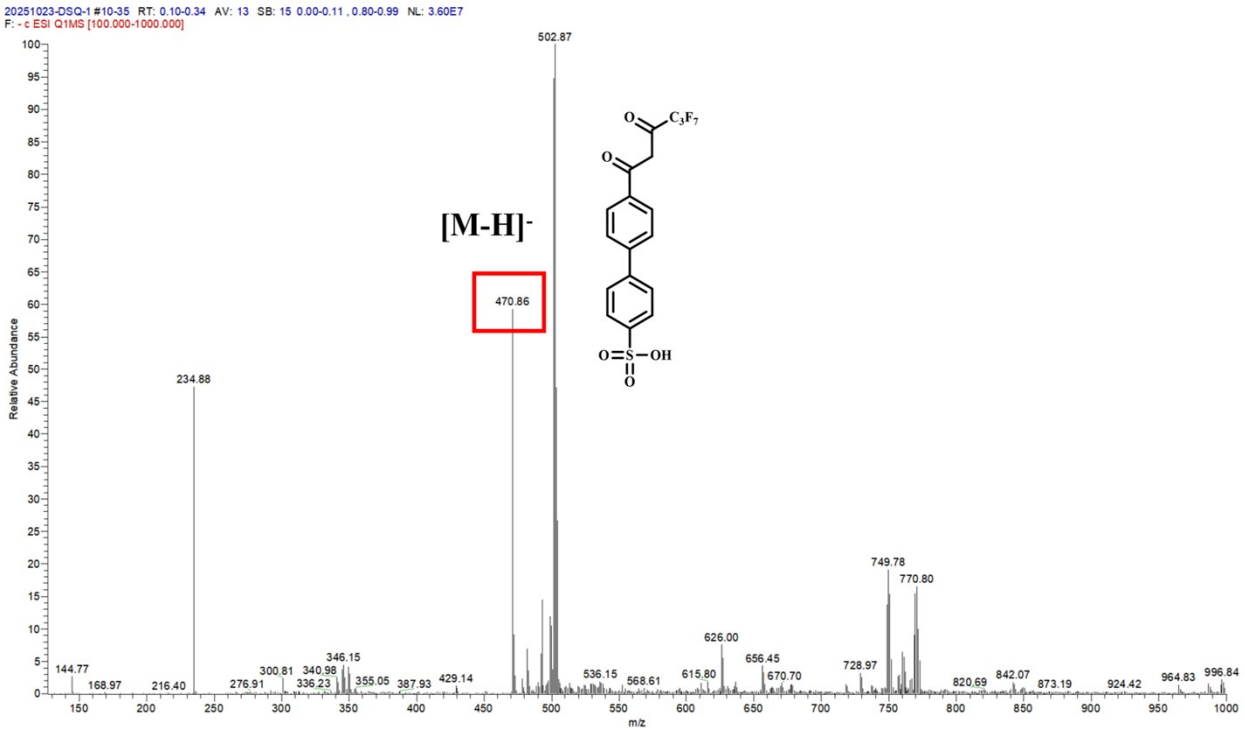

Figure S3. ESI-MS of SDHH.

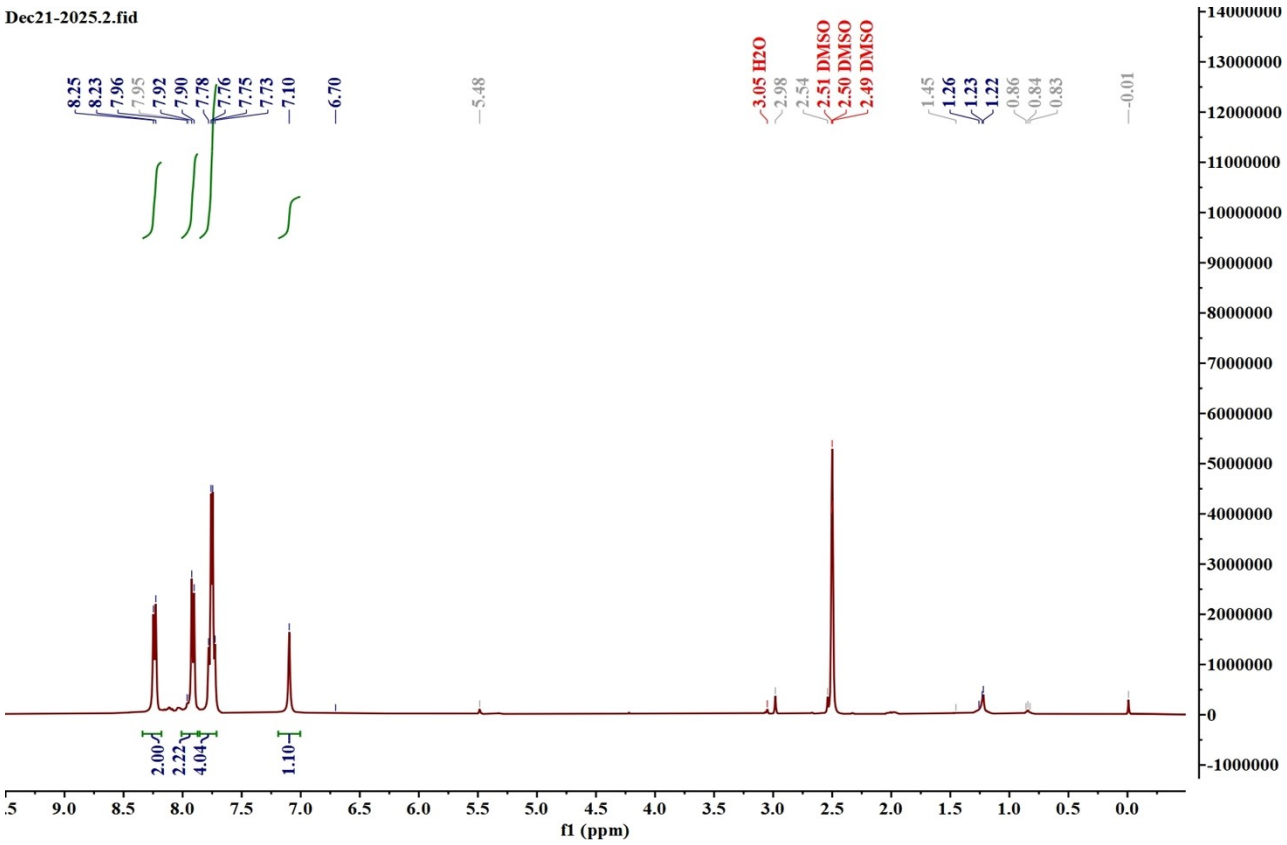

Figure S4. ^{1}H NMR spectrum of SDHH in DMSO-d_6.

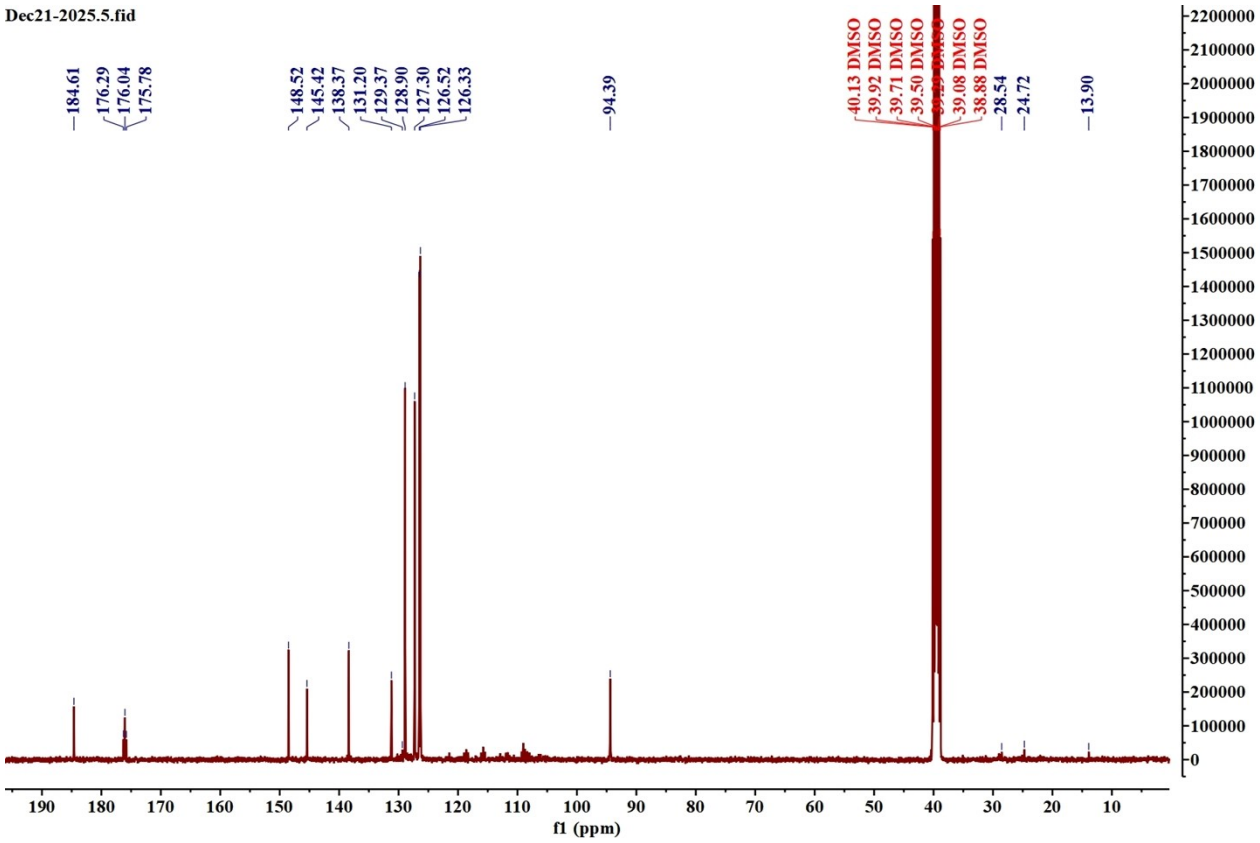

Figure S5. ^{13}C NMR spectrum of SDHH in DMSO-d_6.

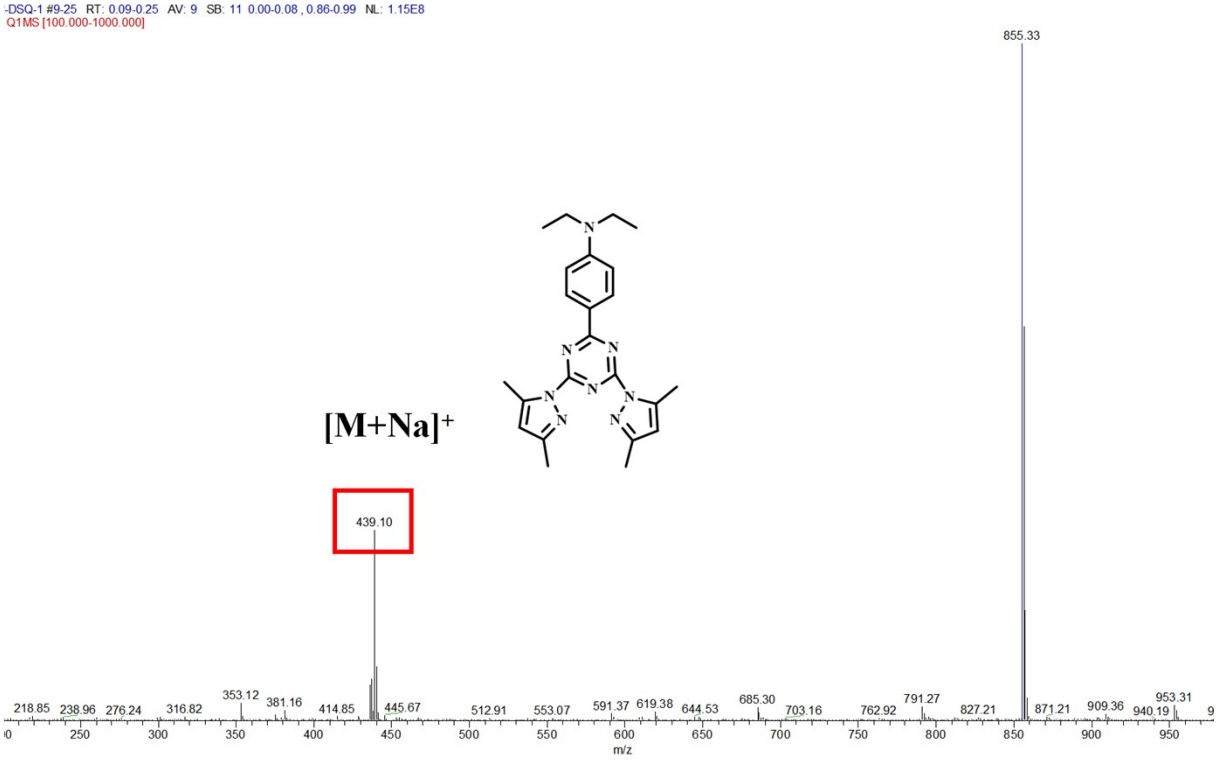

Figure S6. ESI-MS of DPBT.

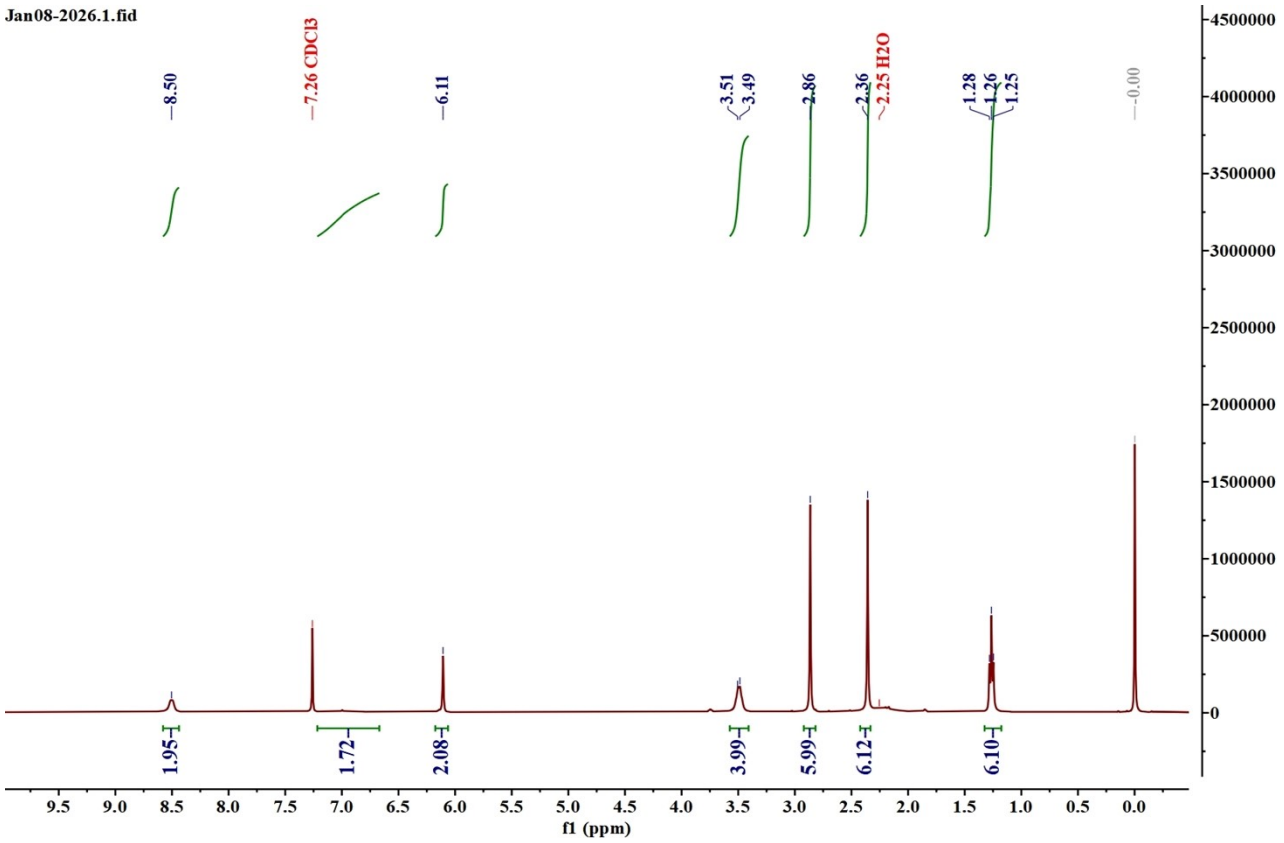

Figure S7. ^{1}H NMR spectrum of DPBT in $CDCl_3$.

3. Characterizations of $Eu(SDHH)_3(DPBT)$ and $Gd(SDHH)_3(DPBT)$

3.1 Synthesis of $Ln(SDHH)_3(DPBT)$

The reaction pathway for the synthesis of **$Ln(SDHH)_3(DPBT)$** is illustrated in **Scheme S2**.

Synthesis of $Eu(SDHH)_3(DPBT)$. A mixture of SDHH (20 mg, 42 μmol, 3 equiv), DPBT (5.8 mg, 14 μmol, 1 equiv), and $EuCl_3 \cdot 6H_2O$ (5.1 mg, 14 μmol, 1 equiv) was dissolved in anhydrous THF (10 mL), followed by the addition of $NaHCO_3$ solution (1 M, 42 μL). The reaction was carried out under an argon atmosphere with reflux for 2 h. After filtration and solvent removal under reduced pressure, the crude product was washed with n-hexane to yield the target complex as a yellow powder (21.2 mg, yield: 76.4%). ESI-MS (m/z): calcd for $[Eu(SDHH)_3(DPBT)\text{-}3H+Na]^{2-}$: 1001.09, found: 1001.10. ^1H NMR (500 MHz, Methanol-*d*4) δ(ppm) = 8.40 (s, 2H), 7.85 (d, J = 7.6 Hz, 4H), 7.47 (s, 4H), 7.11 (s, 2H), 6.83 (s, 1H), 5.80 (s, 2H), 3.55 (s, 4H), 2.99 – 2.77 (m, 4H), 2.68 (s, 6H), 2.41 – 2.31 (m, 2H), 1.26 (s, 6H). HPLC analysis indicated that the purity of the as-synthesized $Eu(SDHH)_3(DPBT)$ complex was 95.33%, demonstrating its high purity for performance studies.

Synthesis of $Gd(SDHH)_3(DPBT)$. The synthesis of the gadolinium complex followed a similar procedure to that of the europium complex, using $GdCl_3 \cdot 6H_2O$ as the metal source. The product was obtained as a yellow powder (21.8 mg, yield: 78.2%). ESI-MS (m/z): calcd for $[Gd(SDHH)_3(DPBT)\text{-}2H]^{2-}$: 992.59, found: 992.60.

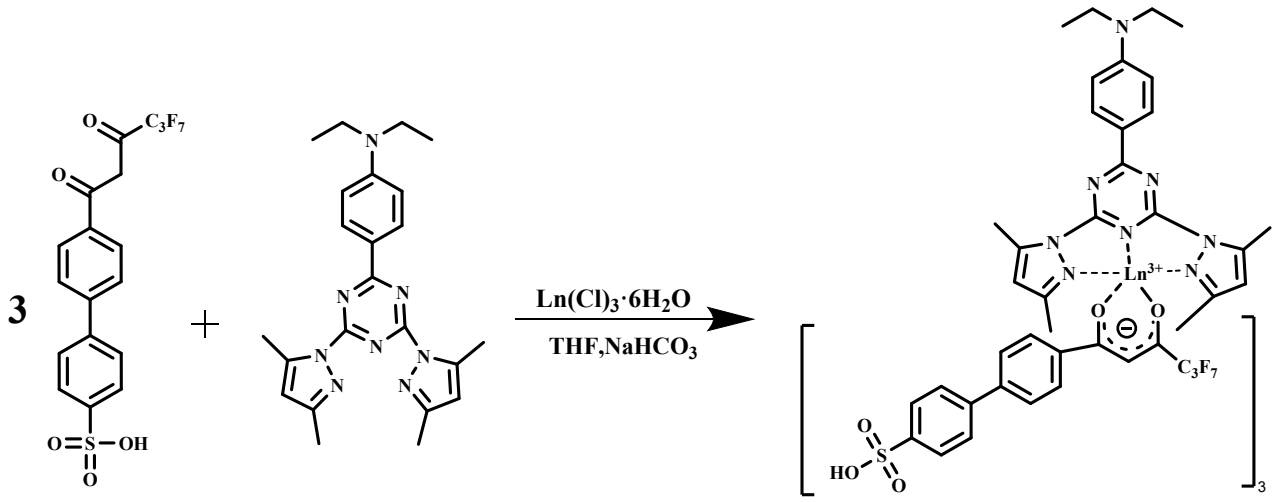

Scheme S2. Reaction pathway for the synthesis of **$Ln(SDHH)_3(DPBT)$**.

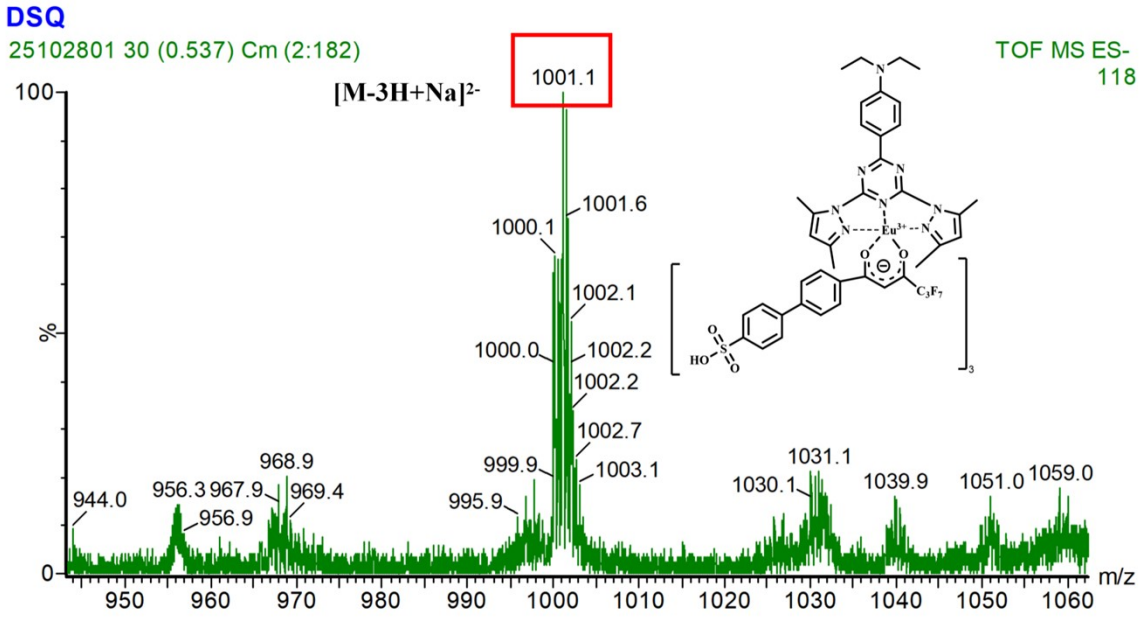

Figure S8. ESI-MS of **Eu(SDHH)$_3$(DPBT)**.

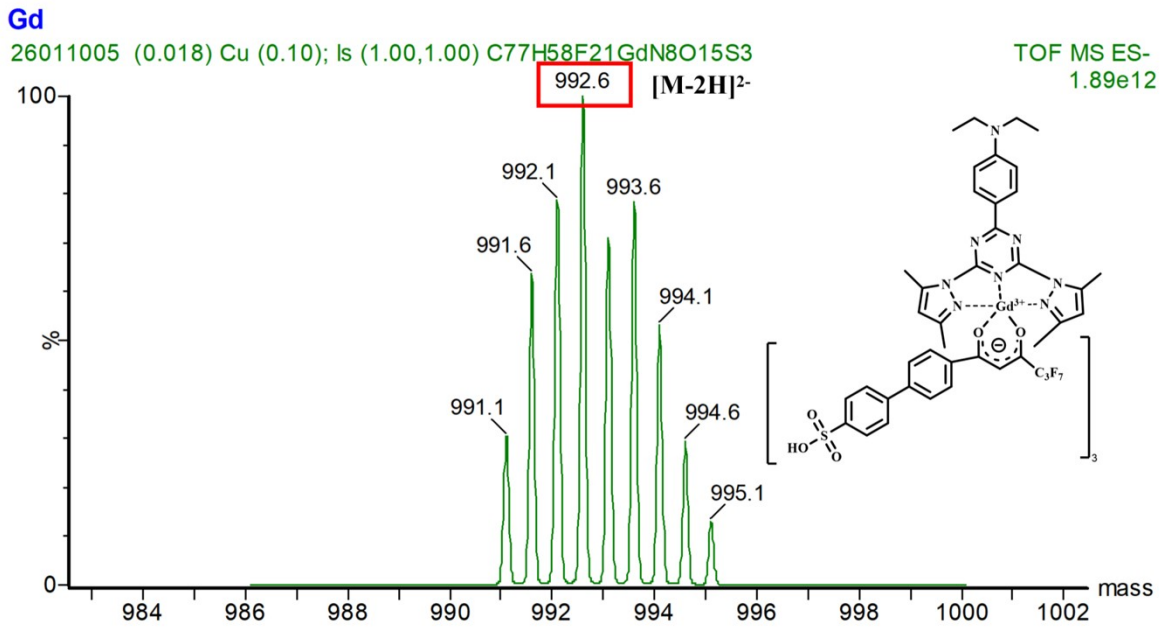

Figure S9. ESI-MS of **Gd(SDHH)$_3$(DPBT)**.

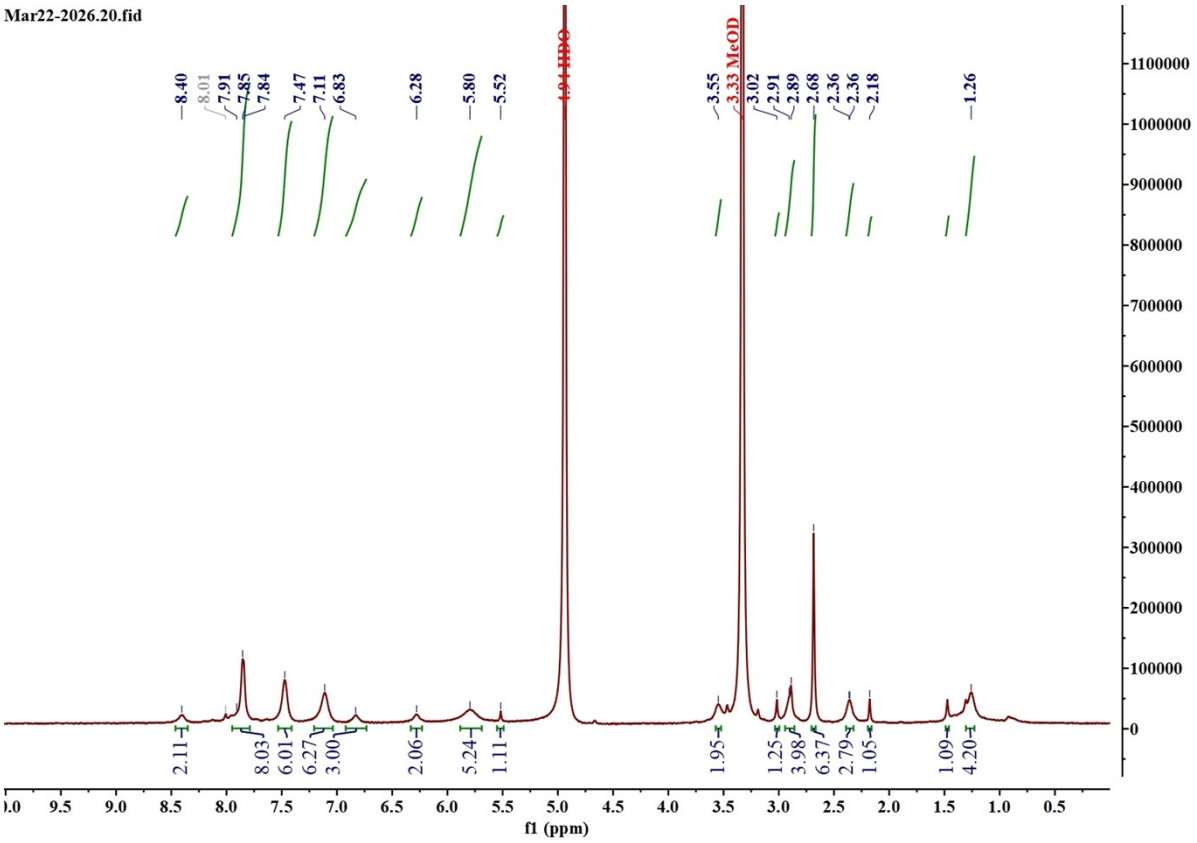

Figure S10. ^{1}H NMR spectrum of **Eu(SDHH)$_3$(DPBT)** in CD_3OD.

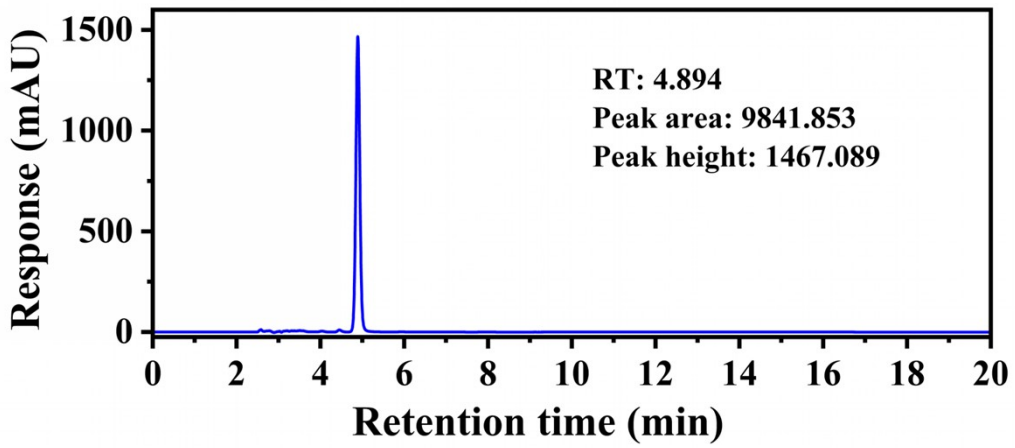

Figure S11. HPLC chromatograms of the synthesized **Eu(SDHH)$_3$(DPBT)** complex (95.33% yield) by ZORBAX 3 μm 4.6 × 150 mm C18 reverse-phase column, using methanol (100%) as the eluent (flow rate, 0.5 mL/min). The elution was monitored at 405 nm.

4. DLS analysis of $Eu(DHH)_3(DPBT)$ and $Eu(SDHH)_3(DPBT)$

Sample description	PDI	Average particle size (nm)
$Eu(DHH)_3(DBPT)$	0.438	2089.9
$Eu(SDHH)_3(DBPT)$	0.347	363.8

Table S1. DLS of **$Eu(DHH)_3(DPBT)$** and **$Eu(SDHH)_3(DPBT)$**

5. Water solubility comparison between $Eu(SDHH)_3(DPBT)$ and $Eu(DHH)_3(DPBT)$

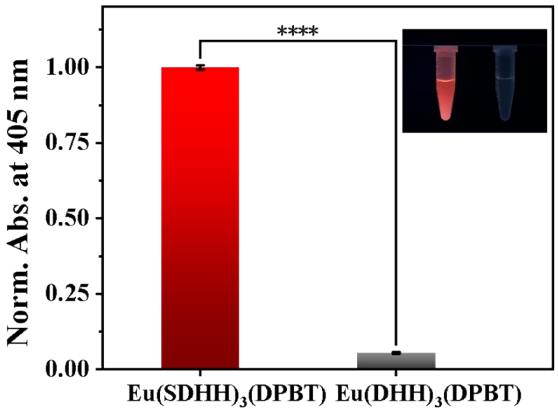

Figure S12. Normalized absorbance of the saturated aqueous solutions of **$Eu(SDHH)_3(DPBT)$** and its non-sulfonated analogue **$Eu(DHH)_3(DPBT)$** at 405 nm (Statistical significance: ****$P <$ 0.0001). Inset: Photographs of the corresponding filtrates under 365 nm UV irradiation.

6. Characterization of the reaction products of $Ln(SDHH)_3(DPBT)$ upon treatment with HClO

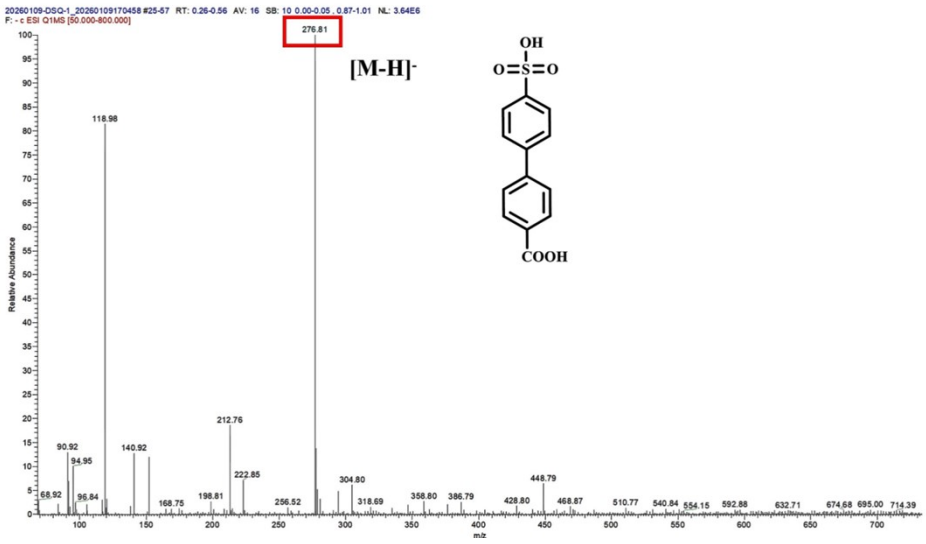

Figure S13. ESI-MS of the reaction products of **$Ln(SDHH)_3(DPBT)$** (10 μM) upon treatment with HClO (50 μM) in 50 mM borate buffer at pH 7.4.

7. UV-vis absorption spectroscopic investigation of $Eu(SDHH)_3(DPBT)$ response toward HClO

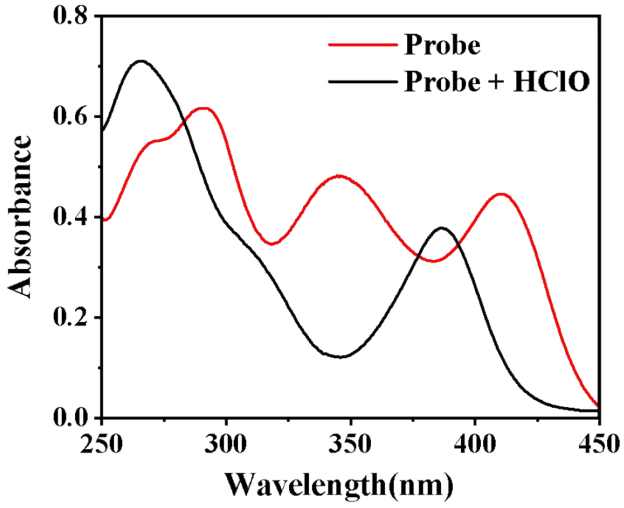

Figure S14. UV-vis absorption spectra of **$Eu(SDHH)_3(DPBT)$** (10 μM) before (red line) and after (black line) reaction with HClO (50 μM) in 50 mM borate buffer (pH 7.4).

8. TGL excitation and emission spectra of $Eu(SDHH)_3(DPBT)$ in the absence and presence of HClO

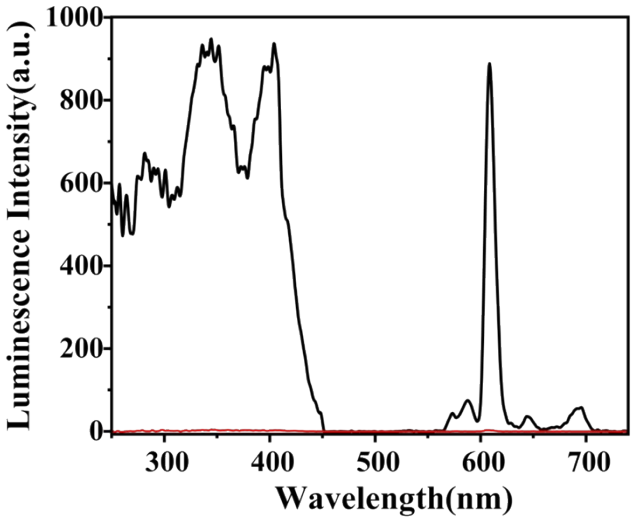

Figure S15. Time-gated excitation and emission spectra of **$Eu(SDHH)_3(DPBT)$** (5 μM) before (black line) and after (red line) reaction with HClO (50 μM) in 50 mM borate buffer at pH 7.4.

9. Effects of pH on the TGL response of $Eu(SDHH)_3(DPBT)$ to HClO

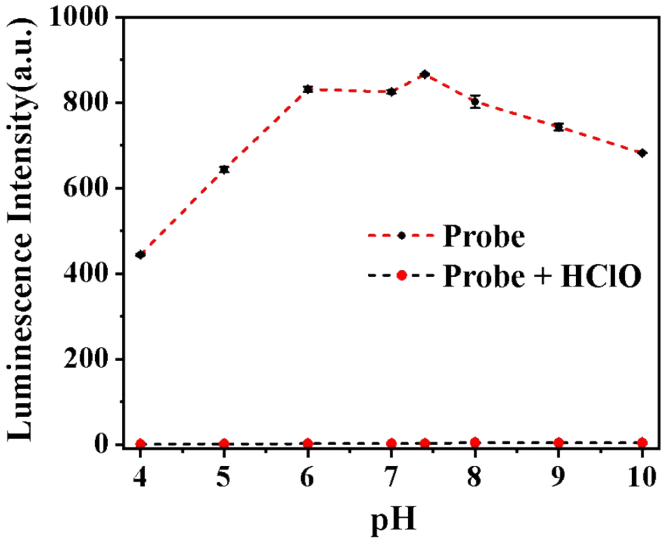

Figure S16. Effect of pH on the TGL response of **$Eu(SDHH)_3(DPBT)$** (5.0 μM) towards HClO (50 μM) in 50 mM borate buffer with different pH values.

10. ^{19}F MR response of Eu(SDHH)$_3$(DPBT) to HClO

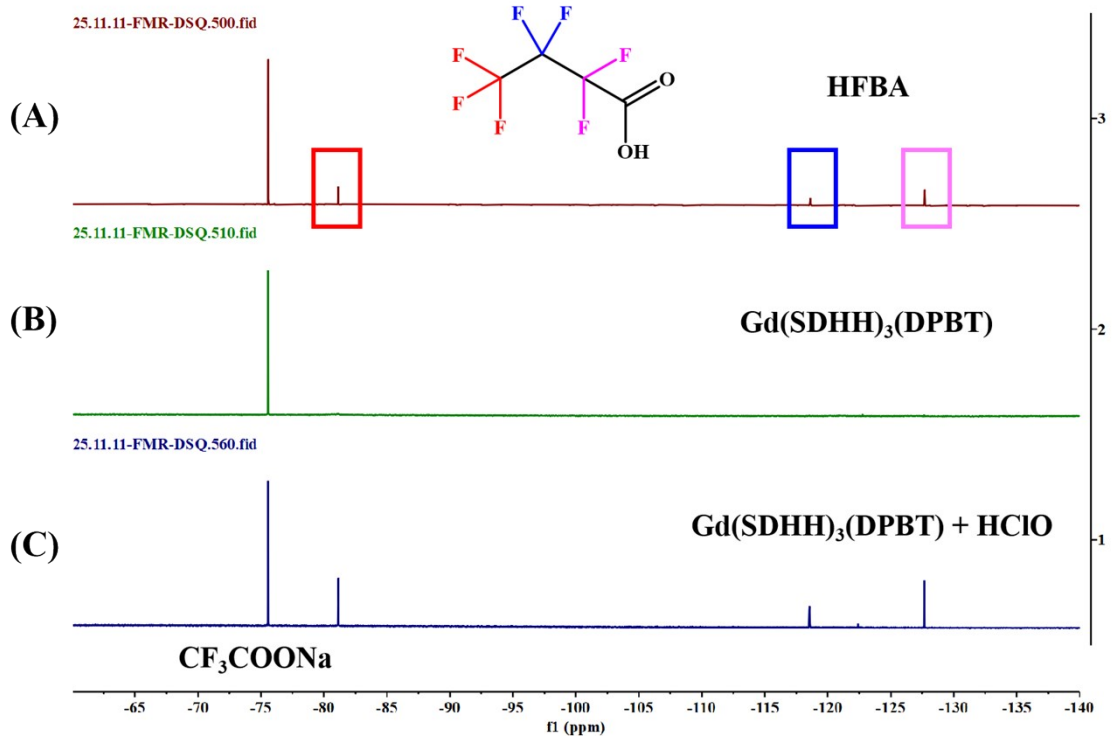

Figure S17. ^{19}F NMR spectra of **Gd(SDHH)$_3$(DPBT)** before and after being reacted with HClO in D_2O using CF_3COONa as an internal reference**.** (A) ^{19}F NMR spectrum of HFBA. (B) The solution of **Gd(SDHH)$_3$(DPBT)** (1.0 mM). (C) The solution of **Gd(SDHH)$_3$(DPBT)** (1.0 mM) reacted with HClO (8.0 mM).

11. Cytotoxicity Assays of $Eu(SDHH)_3(DPBT)$ in Living Cells

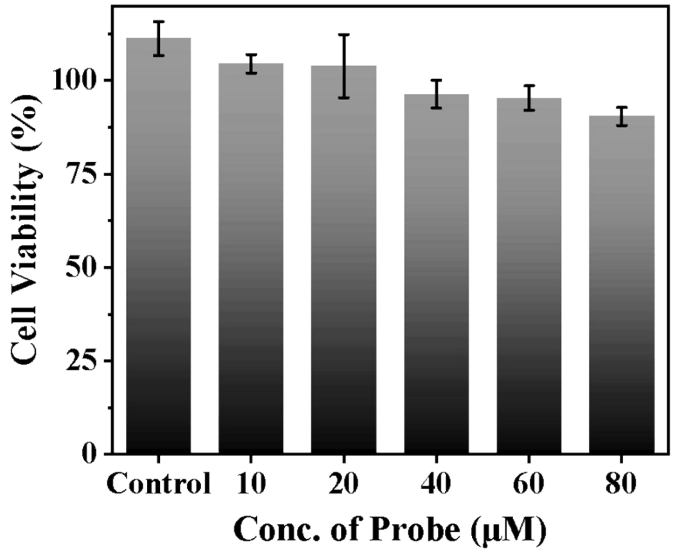

Figure S18. Viabilities of Hela cells incubated with different concentrations of **$Eu(SDHH)_3(DPBT)$** at 37 ℃ for 24 h.

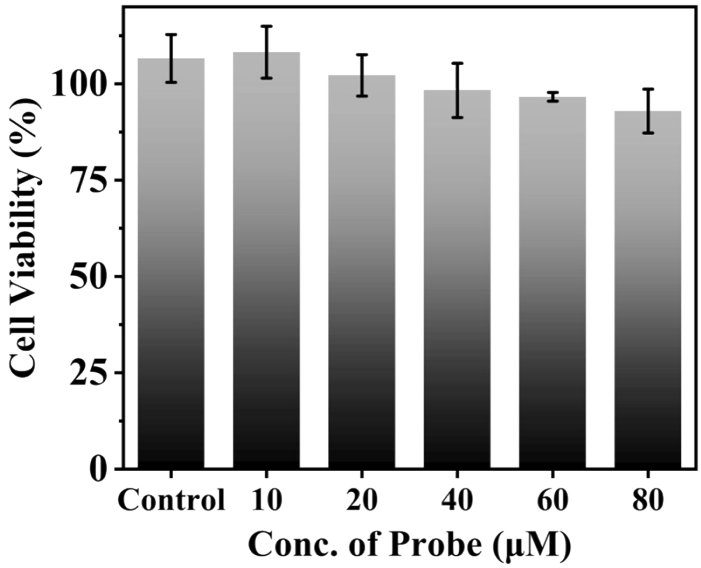

Figure S19. Viabilities of HK-2 cells incubated with different concentrations of **$Eu(SDHH)_3(DPBT)$** at 37 ℃ for 24 h.

12. Luminescence imaging of $Eu(SDHH)_3(DPBT)$ in kidneys of Acute kidney injury mouse models

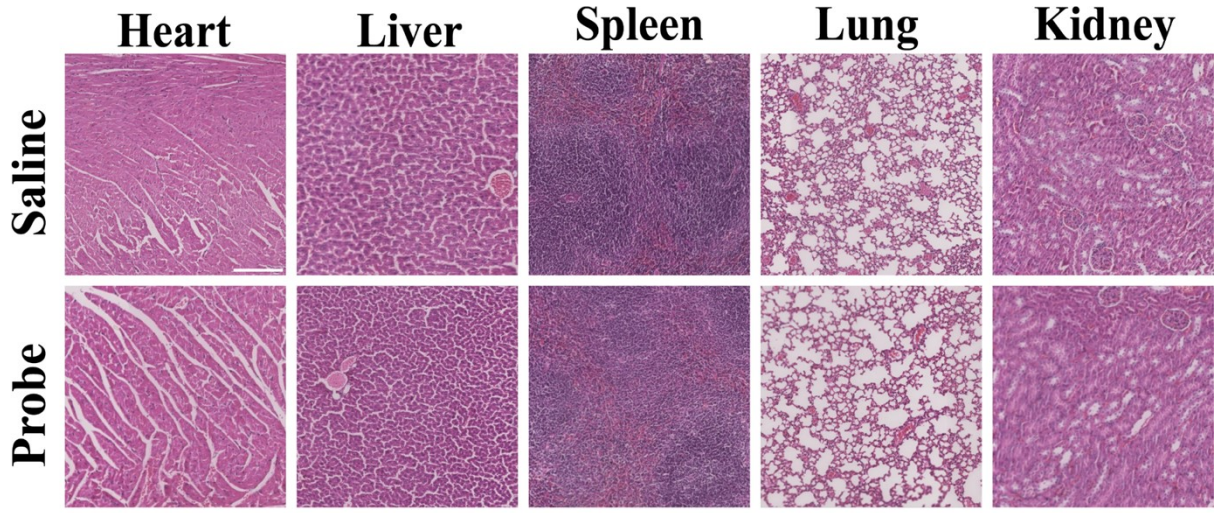

Figure S20. Images of H&E-stained major organ tissues of the mice intravenously injected with saline and **Eu(SDHH)$_3$(DPBT)** (100 μL in physiological saline, 100 μM) for 24h. Scale bar: 200 μm.

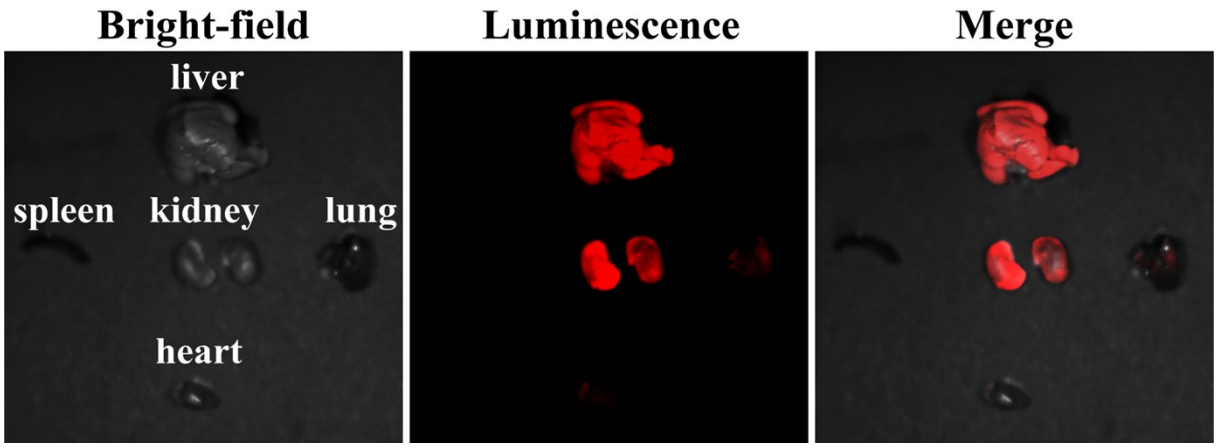

Figure S21. Ex vivo luminescence images of resected organs of the mice after intravenous injection of **Eu(SDHH)$_3$(DPBT)** (100 μL in physiological saline, 100 μM) for 2 h.

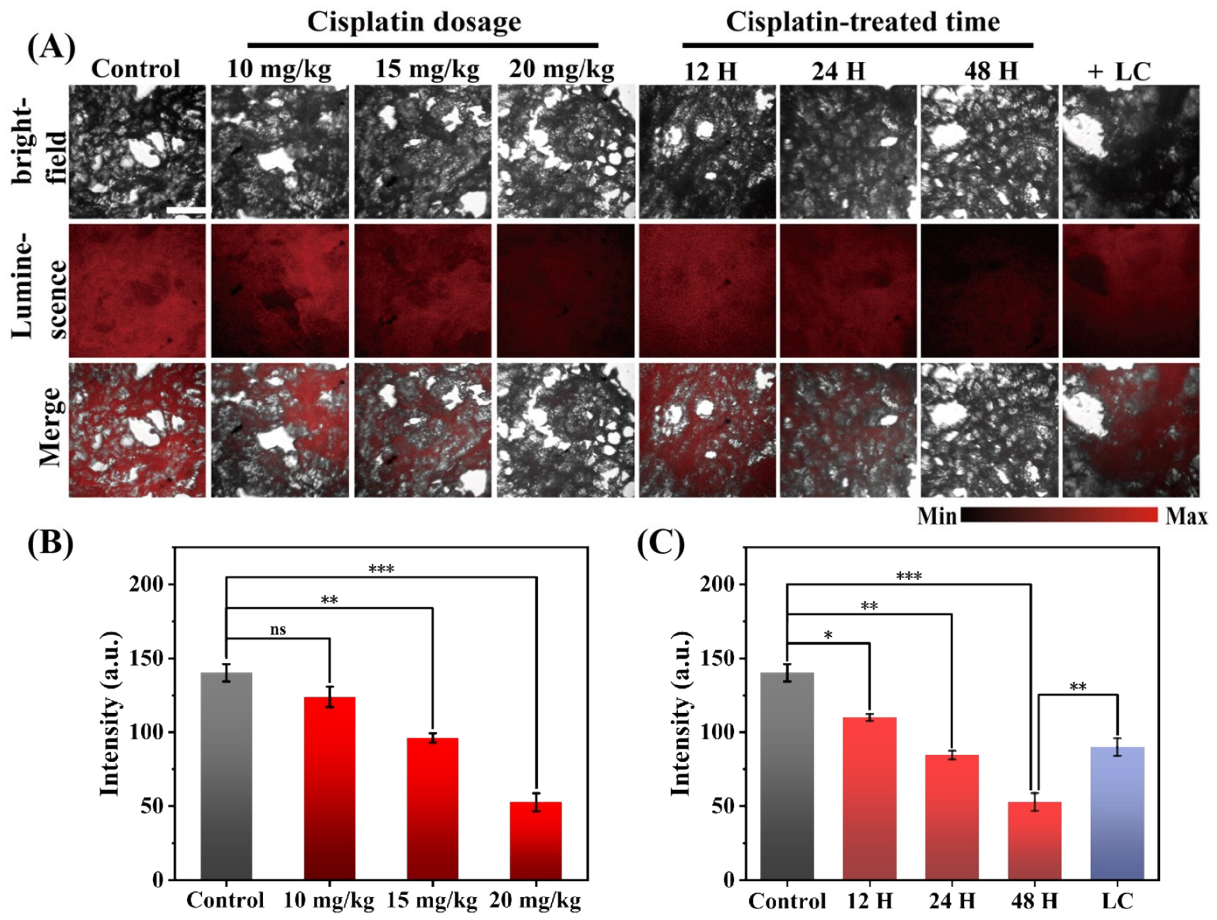

Figure S22. TGL imaging of endogenous HClO in kidney frozen sections from cisplatin-induced acute kidney injury (AKI) mice. (A) Representative TGL images of kidney sections from different groups: Control group; groups treated with different doses of cisplatin (10, 15, and 20 mg/kg) for 48 h; groups treated with cisplatin (20 mg/kg) for different time intervals (12, 24, and 48 h); and the LC protective group (pre-injected with LC (400 mg/kg), then cisplatin for 48 h). After the indicated treatments, all mice were intravenously injected with the probe via the tail vein for imaging. (B) Quantitative analysis of the relative TGL intensity in the kidney sections from mice treated with different doses of cisplatin. (C) Quantitative analysis of the relative TGL intensity in the kidney sections from mice treated with cisplatin for different times and the LC protective group. Data are presented as mean ± SD (n = 3). Statistical significance: $^{**}P < 0.01$, $^{***}P < 0.001$, and ns (no significance) compared with the control group or between specific groups. Scale bars: 100 μm.

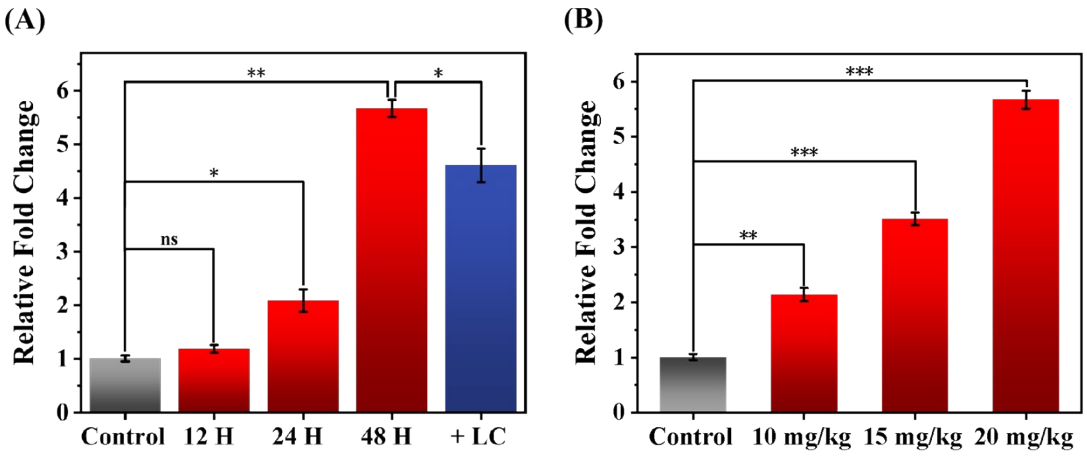

Figure S23. Serum Cr levels (SCr) of mice in different groups. (A) Time-dependent changes in serum Cr levels of mice treated with cisplatin (20 mg/kg) for 12, 24, 48 h and the protective effect of L-carnitine pretreatment (L-carnitine + 20 mg/kg cisplatin). (B) Dose-dependent changes in serum Cr levels of mice treated with different doses of cisplatin (10, 15, and 20 mg/kg) groups. Data are presented as mean ± SD (n = 3). Statistical significance: *$P < 0.05$, **$P < 0.01$, ***$P < 0.001$, and ns (no significance) compared with the control group or between specific groups.

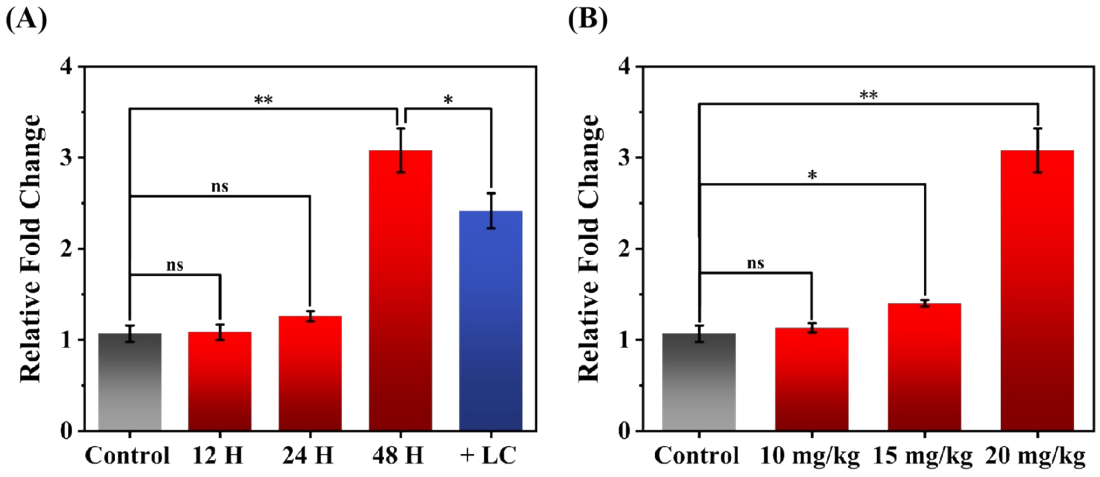

Figure S24. Urea levels of mice in different groups. (A) Time-dependent changes in urea levels of mice treated with cisplatin (20 mg/kg) for 12, 24, 48 h and the protective effect of L-carnitine pretreatment (L-carnitine + 20 mg/kg cisplatin). (B) Dose-dependent changes in urea levels of mice treated with different doses of cisplatin (10, 15, and 20 mg/kg) Data are presented as mean ± SD ($n = 3$). *$P < 0.05$, **$P < 0.01$ compared with the control group; ns: no significance.

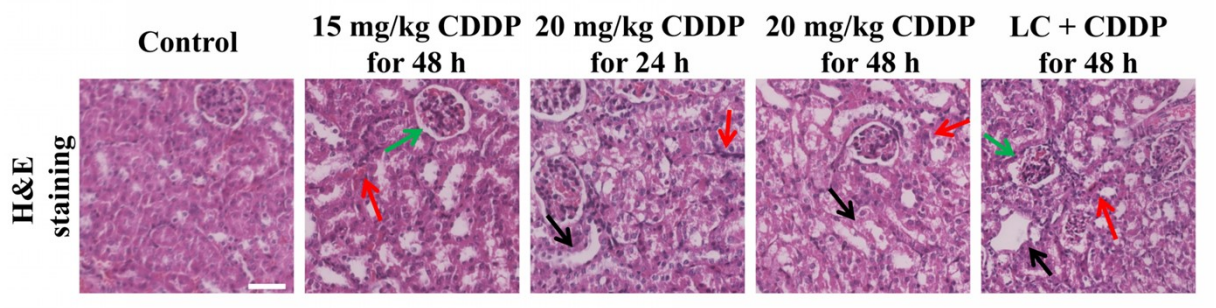

Figure S25. Images of H&E stained kidney tissues from the Control group, Cisplatin-treated group and Therapeutic group. Green: glomerular hypertrophy; Black: hyaline cast formation; Red: tubular cell necrosis. Scale bar: 50 μm.

8. References

1. L. Zhang, X. Zheng, W. Deng, Y. Lu, S. Lechevallier, Z. Ye, E. M. Goldys, J. M. Dawes, J. A. Piper and J. Yuan, *Sci. Rep.*, 2014, **4**, 6597.
2. G. Wang, J. Yuan, K. Matsumoto and Z. Hu, *Anal. Biochem.*, 2001, **299**, 169-172.
3. J. Wu, Y. Yang, L. Zhang, H. Wang, M. Yang and J. Yuan, *J. Mater. Chem. B*, 2017, **5**, 2322-2329.